4-28-2022

Tesing Cababilities of Proposed Telescope Lynx through Simulated Bubbles in the Intracluster Medium

Sierra Rose Hauck

Testing of the Capabilities of Proposed Telescope Lynx through Simulated Bubbles in the Intracluster Medium

by

Sierra Rose Hauck

An Honors Capstone

submitted in partial fulfillment of the requirements

for the Honors Bachelor's Degree

to

The Honors College

of

The University of Alabama in Huntsville

April 28th, 2022

Honors Capstone Director: Dr. Stephen Walker

Assistant Professor of Physics at The University of Alabama in Huntsville

Sierra Hauck 4 / 28 / 2022

Student Date

SAWalker 4/28/2022

Director Date

JAM James Miller
cn=James Miller, o=UAH, ou=PH & ISEd,
email=millerja@uah.edu, c=US
2022.04.29 09:48:10 -05'00'

Department Chair Date

William Wilkerson Digitally signed by William Wilkerson
Date: 2022.04.29 15:36:38 -05'00'

Honors College Dean Date

HONORS COLLEGE
THE UNIVERSITY OF ALABAMA IN HUNTSVILLE

Honors College
Frank Franz Hall
+1 (256) 824-6450 (voice)
+1 (256) 824-7339 (fax)
honors@uah.edu

Honors Thesis Copyright Permission

This form must be signed by the student and submitted as a bound part of the thesis.

In presenting this thesis in partial fulfillment of the requirements for Honors Diploma or Certificate from The University of Alabama in Huntsville, I agree that the Library of this University shall make it freely available for inspection. I further agree that permission for extensive copying for scholarly purposes may be granted by my advisor or, in his/her absence, by the Chair of the Department, Director of the Program, or the Dean of the Honors College. It is also understood that due recognition shall be given to me and to The University of Alabama in Huntsville in any scholarly use which may be made of any material in this thesis.

Sierra Rose Hauck

Student Name (printed)

Sierra Hauck

Student Signature

4/28/2022

Date

1 Table of Contents

2 Abstract

The goal of this project was to test the ability of proposed x-ray telescope Lynx to observe dim extragalactic phenomena. To conduct this examination, we simulated rising plasma bubbles in the intracluster medium, which are thought to be caused by the jets of Active Galactic Nuclei [AGN]. Simulations were passed through Simx, a program designed to emulate the quality of images produced by telescopes. Statistical and qualitative analysis on the images followed, with the goal of determining if simulated bubbles remained visible under a variety of conditions. Conditions tested included exposure times, orientation of bubbles with respect to the viewer, and distance between bubbles and the center of the cluster.

3 Background

Lynx is a proposed next-generation x-ray observatory, one of four missions to have been placed under consideration in the NASA 2020 Decadal Survey. The proposed observatory would be composed of a series of grazing incident mirrors with an outer diameter of 3m and an effective area of $2m^2$ at 1 keV. Instruments on board the observatory include a High-Definition X-ray Imager [HDXI], which would feature a pixel size of less than 0.5 arcseconds, a 20 x 20 arcsecond field of view and a spectral resolution of 100 eV from 0.1 – 10 keV. This instrument would improve massively upon the capabilities of currently available technology – compared to a modern x-ray telescope such as Chandra, Lynx would provide 50x greater throughput, would be able to maintain its spatial resolution 16x farther out, and could survey the x-ray sky 800x faster [Gaskin et al., 2019].

One area in which Lynx's improved technology may prove greatly beneficial is the continued research of "the cooling flow problem," which has dominated the study of galaxy clusters in the past two decades. The nature of the problem is as follows: research from individuals such as McNamara & Nulsen [McNamara and Nulsen, 2007] has shown that that gas in the cores of galaxy clusters have cooling times significantly shorter than their age – in some cases being as low as 3 Gyr [Dunn and Fabian, 2006]. If these gasses were allowed to cool uninhibited, we would expect to see massive growth in the stellar masses of most galaxy clusters at this point in time. Observations of clusters have shown some moderate rate of star formation - the highest being in A1835, which possesses a rate of $\sim$125 $M_\odot$ yr^{-1}. However, even in this extreme example, the rate of stellar formation does not equal the mass cooling rate – estimated for A1835 to be $1000M_\odot$ yr^{-1} [Fabian, 2012]. This discrepancy points towards the existence of a heat source somewhere within the cluster which prevents the gas from effectively cooling.

Of all candidate heat sources, the most popular in recent literature is an AGN at the the center of the Brightest Cluster Galaxy [BCG]. It is proposed that infalling matter, in the form of ionized plasma, may generate magnetic field lines around the supermassive black hole, which may in turn cause the formation of large radio jets which serve to blow hot matter into the intracluster medium [Diehl et al., 2008]. Several steps of this process have already been observed by astronomers; almost all BCG AGN have been shown to have an active radio-loud source, and the majority of clusters - 95%, as of 2012 - with cooling times of less than 3 Gyr have been shown to have associated cavities once projection effects are considered [Fabian, 2012]. Some examples of these cavities, taken from observations by Chandra, are shown below:

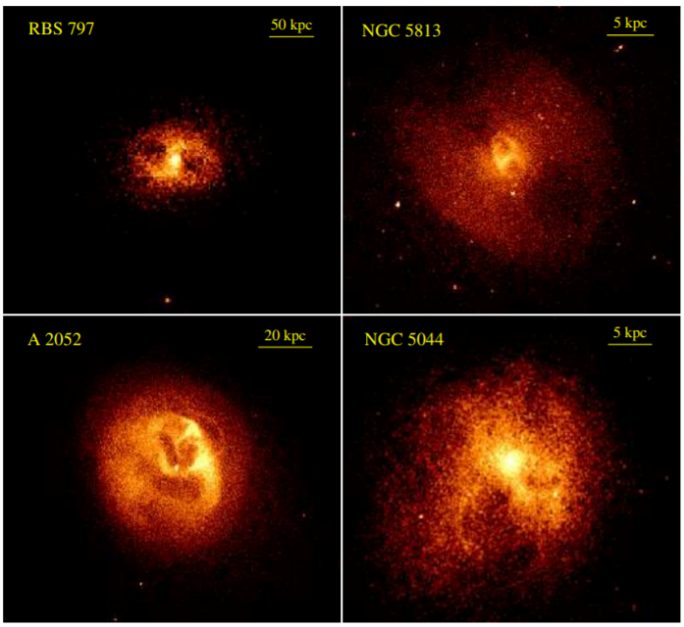

Figure 1: Chandra X-Ray images showcasing the interaction between BCG AGN and the surrounding intracluster medium. [Fabian, 2012]

Notable efforts to constrain the nature of these cavities include the work of Steven Diehl and Hui Li in 2008, who by analysing multiple cavity-containing clusters were able to determine that there existed a powerlaw relationship between the radius of cavities and their distance from the center of the cluster. This relationship is showcased by the following plot:

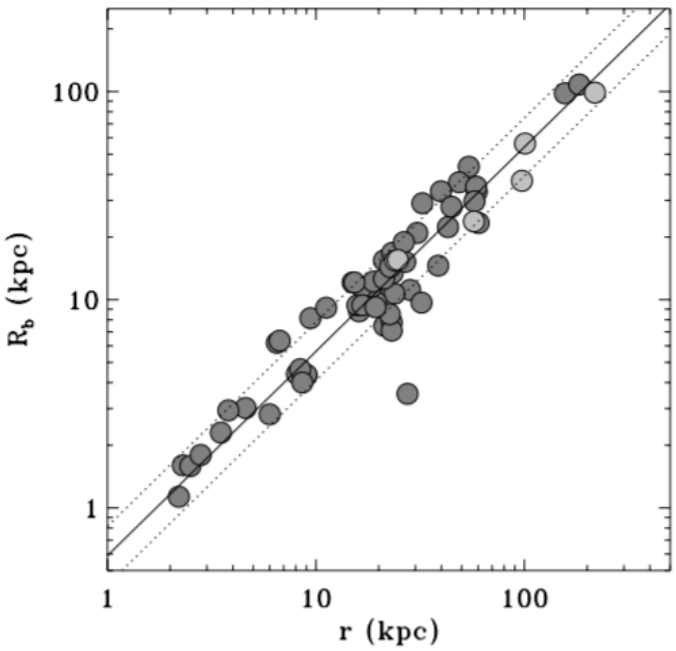

Figure 2: A chart comparing radius of the cavities of multiple clusters to their respective distance from the center of their host clusters. Note the powerlaw model that emerges when both parameters are plotted in

log scale. [Diehl et al., 2008]

Currently, further investigation of these clusters is held back by a lack of spatial and spectral resolutions at key wavelengths, both of which are required to accurately map the ways in which jets interact with the surrounding intracluster medium. It is in solving this issue that next-generation telescopes such as Lynx may prove vital for future studies.

4 Investigation

4.1 Overview of Tools Used For Analysis

First, a galactic cluster is simulated using a spherical extended source placed in a 3D IDL environment. Typically, a hydrostatic isothermal model is used to describe the surface brightness profiles of rich clusters. [Mulchaey, 2000]. Following these practices, we utilize a modified version of the standard beta model for our surface brightness calculations. Our model in particular is the result of two standard beta models being added together. This is yet another common practice, and stems from the fact that singular beta models tend to be a poor fit for galaxy clusters; particularly at the center, where an excess of emission is observed [Mulchaey, 2000]. Parameters for our beta model were selected from observations of ABEL 133 by Vikhlinin et al. in 2005, shown in the below figure:

TABLE 2
BEST FIT PARAMETERS FOR GAS DENSITY PROFILES

Cluster	r_{det}[a] (kpc)	n_0 10^{-3} cm^{-3}	r_c (kpc)	r_s (kpc)	α	β	ε	n_{02} 10^{-1} cm^{-1}	r_{c2}	β_2	*ROSAT*[b]
A133	1100	2.968	142.7	1423.3	0.996	0.575	5.000	0.276	33.44	0.980	+
A262	450	3.434	45.2	350.8	1.674	0.333	1.806	...	...	...	+
A383	800	7.000	115.2	422.3	2.018	0.583	0.740	1.014	0.08	1.000	...
A478	2000	8.169	177.1	3148.2	1.493	0.715	5.000	0.584	24.00	1.000	+
A907	1300	6.257	136.9	1885.1	1.554	0.594	4.986	...	...	...	...
A1413	1800	5.526	186.3	2077.1	1.217	0.651	4.991	...	...	...	...
A1795	1500	14.993	72.8	1030.8	1.060	0.545	3.474	...	...	...	+
A1991	1000	9.373	44.4	998.2	1.516	0.501	5.000	0.999	5.00	1.165	+
A2029	2250	16.469	80.7	870.6	1.131	0.539	1.650	3.741	5.00	1.000	+
A2390	2500	3.069	353.6	1200.0	1.917	0.696	0.240	...	...	...	...
RXJ 1159+5531	600	0.198	613.8	961.5	1.762	1.215	4.939	0.416	12.66	1.000	...
MKW4	550	0.280	488.6	1081.6	1.628	1.224	0.000	0.189	11.08	0.661	+
USGC S152	300	17.450	8.1	467.5	2.644	0.453	3.280	...	...	...	...

NOTE. — Derived densities and radii scale with the Hubble constant as $h^{1/2}$ and h^{-1}, respectively.

[a]— The radius (kpc) where X-ray brightness is detected at > 3σ, or the outer boundary of the *Chandra* field of view, whichever is smaller.
[b]— Those clusters for which we use also *ROSAT* PSPC surface brightness measurements.

Figure 3: Table of beta model parameters as observed from various galactic clusters. [Vikhlinin et al., 2006]

ABEL 133 in particular was selected for this experiment because the cluster is relatively simplistic and roughly spherically symmetric. This made it ideal for the construction of models without necessitating a very complex simulation.

Once a source has been generated using the above parameters, two spheroids are subtracted from the model in order to simulate intracluster cavities. A number of simplifications were made for these cavities in order to keep simulation times reasonably low - across all experiments, these cavities are identical in shape, equidistant from the center of the source and lay on an axis which includes both cavities and the center of

the source. Unless otherwise specified, this axis is oriented along the Y axis on the YZ plane – this corresponds to a line-of-sight angle of 90°. An image illustrating this coordinate system will be provided later in this section, when DS9 is discussed. Following the work of Diehl & Li, the radius of each cavity was set to be dependant on its distance to the center of the galactic cluster using the function $r_b = 0.6 * r^{0.96}$. This function was derived directly from the plot shown in the previous section.

Once cavity generation is completed, the image is flattened into a 2D projection and saved as a .fits file. This file is then fed into a program called 'Simx'. Simx is designed to simulate real observations by mimicking the response of detectors onboard various missions [Yamaguchi et al.,]. The following parameters were input into Simx:

- Pointing RA/DEC: This input set the coordinates of the center of the output image. This was matched to the same position as the center of the input image, the location of which was checked by inputting the model into DS9.
- Exposure Time: This input set the amount of time, in seconds, the telescope was allowed to observe the source. This variable was modified as per the needs of specific experiments.
- SourceFlux: This input set the total flux of the source in units of $erg * cm^{-2} * s^{-1}$. This variable was set to a constant $5 * 10^{-11}$ across all experiments, a value which modeled the flux of galactic cluster PKS 0745-191 as observed by Edge et al. in 1990 [Edge et al., 2000]. We selected this cluster in particular due to its redshift of 0.1, which placed it at an ideal distance for Lynx's 20 x 20 arcminute field of view.
- SourceSpectrumType: This input determined whether or not the simulation will use a user-created spectrum file in order to model the energy of its photons. For the sake of simplicity, we decided not to do so in this experiment, and set this parameter to 'Mono'. The selection of Mono assumes that the spectrum is MonoEnergetic; I.E. that all photons from the source have the same amount of energy.
- MonoEnergy: This input set the energy of each monoenergetic photon. We chose to set each photon to an energy of 1 keV, an energy level at which Lynx maintains its $2m^2$ effective area.
- RandomSeed: This input determined whether or not the sequence of random numbers produced for each simulation was randomized each time the simulation ran. We set this to a value of '0', thus opting out of randomization.
- MissionName: This input determined which mission Simx chose to emulate. We selected Lynx.
- InstrumentName: This input determined which of the various instruments onboard Lynx would be emulated. We selected the HDXI instrument.
- ScaleBkgnd: This input determined how the background noise would scale on the image. We set this to a value of '1.0', allowing the background to scale linearly.

Simx outputs an evt.fits file, which can be interpreted by an image processing software such as DS9. In DS9, a gaussian smooth is applied to the images in order to increase the visibility of the cavities. Unless otherwise specified, the smoothing had parameters of $r = 3$, $\sigma = 1.5$. After smoothing, data is extracted from the simulated observations through the use of Pie And Annulus [PANDA] regions. Two regions, identical in size and shape, are applied to each image. One is overlapped with either of the cavities, and the other is oriented perpendicularly such that it contains as little of the cavities as possible. This second region is treated as 'background' data in later analysis.

The bin size of these regions was allowed to vary up to a maximum size of 2 arcseconds per annulus, as some images were particularly large. However, a general effort was made to keep the bin size as close to 0.5 arcseconds per annulus as possible. This size approaches the resolution of one pixel in the simulated images, and keeping our bins close to this size helped to keep errorbars reasonably small. Radius of the regions similarly varied as needed, but regions were generally started at the center of the cluster and extended such that there was some amount of data from behind the cavity. Once regions were properly overlaid on the image, radial profiles were generated and saved in a .dat format. An example image showing both PANDA regions and the coordinate system is provided below:

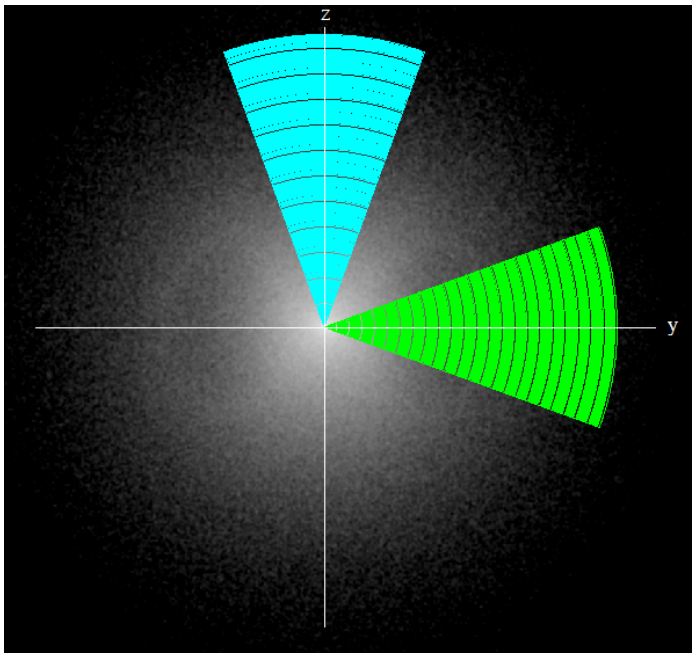

Figure 4: Example cavity simulation including DS9 PANDA regions. Green corresponds to the region containing a cavity, while blue corresponds to background data. Also note the inclusion of axes – the x axis can be assumed to be coming out of the page.

The last step in analysis is to export these .dat files into Veusz, a python-based plotting package. Residuals of each source are created by subtracting the counts of the background region from the cavity region - due to the way the models were originally constructed, is the rough equivalent to fitting the data with a beta model. Residuals are then plotted against the radius of the region – since each region started at the center

of the image, this is roughly equivalent to the radius from the center of the cluster. If a cavity is detected with statistical significance, we expect to see a sharp dip into 'negative counts' in the relative surface brightness on the y axis of the plot. This implies that the cavity is dimmer than the background – as we would expect, as these cavities are regions of lower intracluster medium density and thus emit fewer photons.

4.2 Impact of Exposure Times

For this experiment, simulations were run for a cavity distance of 100 kpc. Exposure times in Simx were allowed to vary between 2 – 16 ks, and PANDA regions were given a bin size of 0.5 arcseconds per annulus.

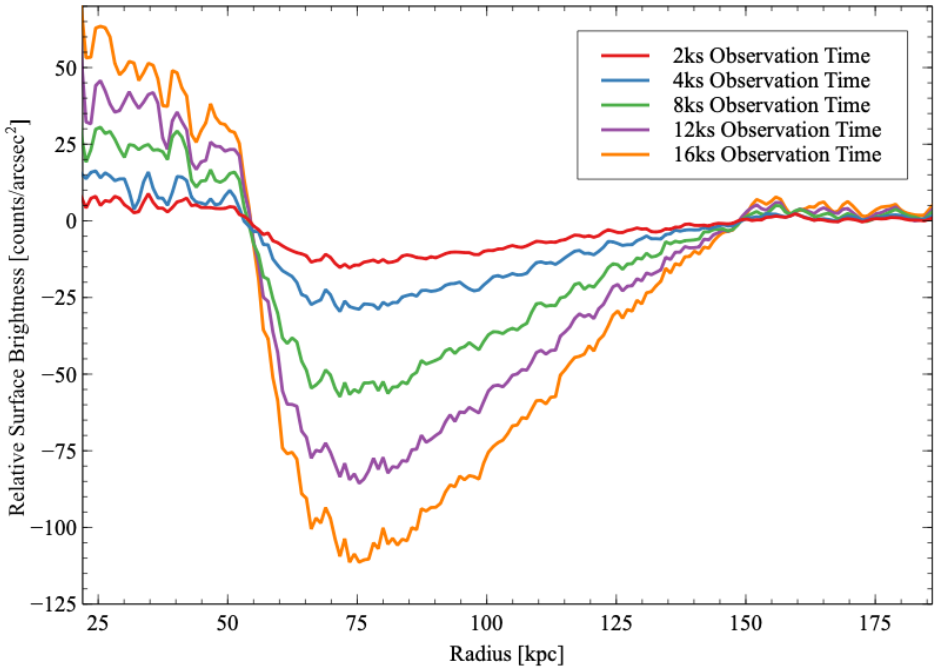

Figure 5: Residuals of cavities with exposure times ranging between 2 - 12 ks. Note the roughly linear rate of decrease in the minimum relative surface brightness.

As expected, higher exposure times resulted in a larger magnitude in the relative surface brightness between the cavity and background data. Notably, the relationship between the minimum relative surface brightness and the exposure time appears to be linear, with each ks of observation time corresponding to an increase in the minimum relative surface brightness of roughly 6.78 counts.

Based on these observations, we can predict that cavities at this particular distance and orientation may be visible with a minimum observation time of ∼147s. Below this point, estimates suggest that the magnitude of the minimum relative surface brightness would fall below a one-count difference; at this point, the source would be unobservable even under ideal conditions. For the study of cavities at larger distances and non-ideal orientations to the line-of-sight, we predict that an observation time of 4ks may provide useful data. This prediction will be tested in later experiments.

4.3 Impact of Cavity Distance to Center of Galactic Cluster

In this experiment, simulations were run for cavity distances ranging from 100 – 400 kpc, while exposure times were set in Simx at a fixed value of 10ks. Bin sizes had to be adjusted to accommodate cavity sizes at large distances; 0.5 arcseconds per annulus was utilized for the 100 kpc trial, and a further 0.5 arcseconds were added for each increase of 100 kpc from the cluster center.

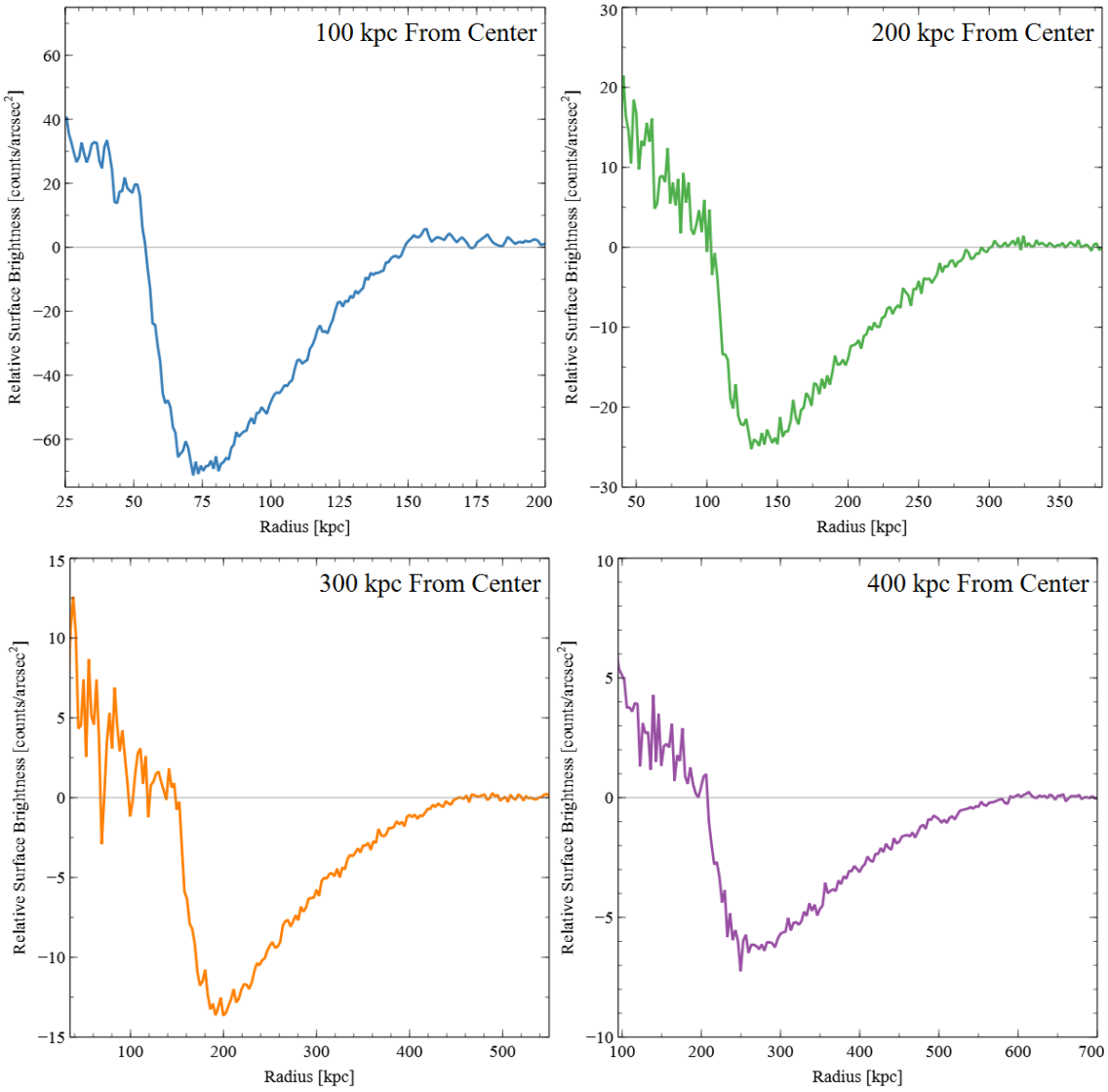

Figure 6: Residuals of cavities centered 100, 200, 300 and 400 kpc from the center of the galactic cluster. Note the gradual decrease in magnitude of the observation.

As the center of the cavities progressed further from the cluster center, the magnitude of the relative surface brightness decreased as expected. As in the previous experiment, we attempted to extrapolate this data to larger distances by plotting the minimum relative surface brightness against the distance to the cluster center. The plot on the following page resulted:

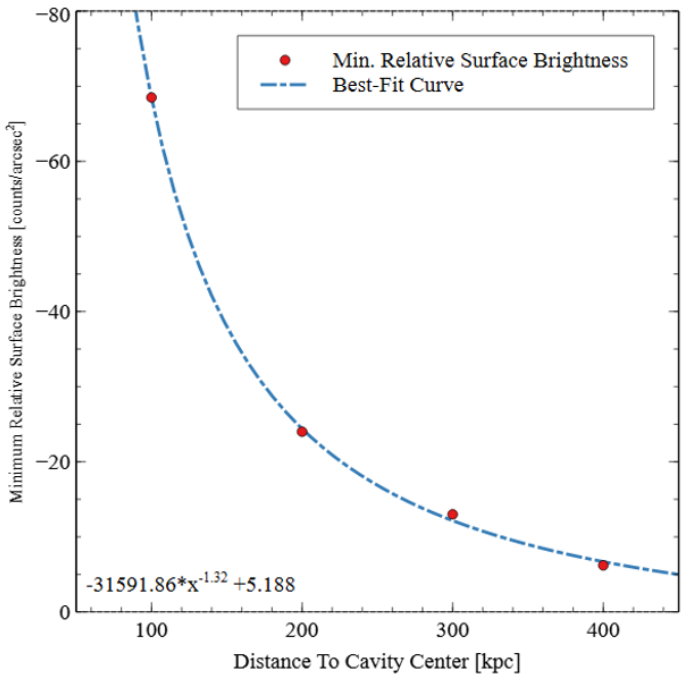

Figure 7: Plot of minimum relative surface brightness against distance from cavity to center of the galactic cluster. Note the powerlaw model that emerges.

Notably, a powerlaw model provided a reasonably good fit for our data set. Based on this data, we can infer that 10 ks of exposure time may permit the detection of cavities to ∼650 kpc; beyond this point, the magnitude of the relative surface brightness would once again fall below one count.

4.4 Impact of Cavity Orientation

For this experiment, simulations were run with a cavity distance of 100 kpc, a bin size of 0.5 arcseconds per annulus and an exposure time of 4 ks. In order to test the impacts of projection on cavity visibility, cavities was allowed to rotate about the z axis, shifting gradually from the y axis towards the line-of-sight.

Angles of rotation between 40°and 80°from the y axis were tested. As rotation increased, the cavities would first appear to get closer to the center of the image in DS9; then, as rotation surpassed 60°, the cavities appeared to overlap. This effect is demonstrated below:

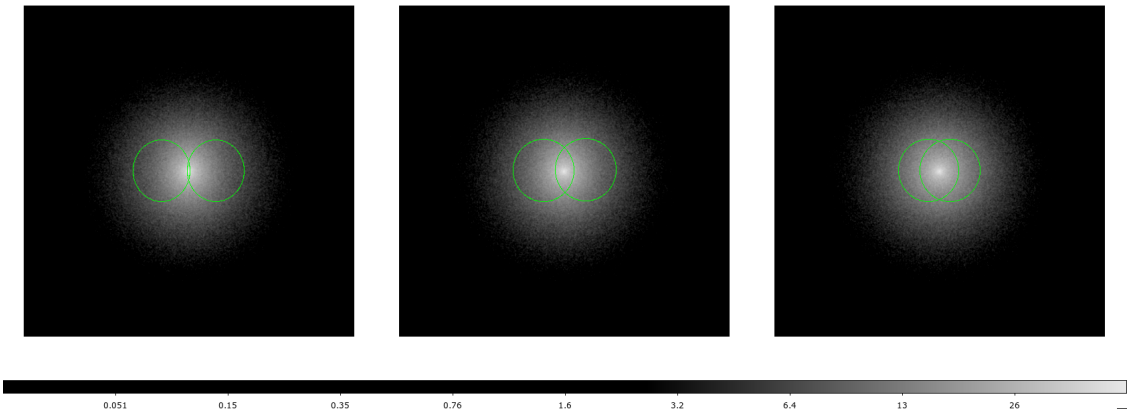

Figure 8: Left: Cavities with 60°rotation. Middle: Cavities with 70°rotation. Right: Cavities with 80°. Note the increasing overlap of the cavities as the angle rotation is increased.

In our residual plots, this corresponded with two separate trends. First, cavities appeared to be centered closer to the cluster center than expected, with higher angles of rotation corresponding to slightly lower apparent cavity distances. Second, cavities with rotations in excess of 60°appeared to be underestimated in size. This was likely a result of the manner in which we collected our background data, as high levels of alignment with the line-of-sight would result in some amounts of cavity being present in background regions. It remains untested if this underrepresentation would persist if more traditional methods of data fitting, such as the construction of a beta model fit in Veusz, were utilized.

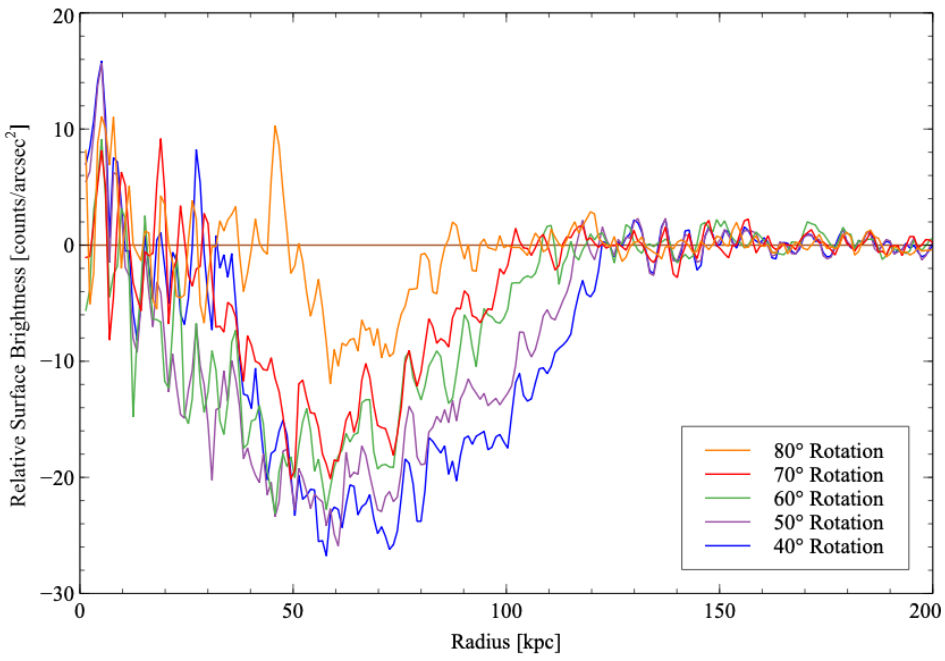

Figure 9: Residuals of cavities ranging between 40 and 80 degrees of rotation. Note the sharp decrease in significance between 70 and 80 degrees of rotation.

Beyond the two trends outlined above, it should be noted that higher angles of rotation corresponded generally to lower magnitudes in observations, with an especially prominent rate of decrease between 70°and 80°of rotation. This is likely due to the brightness of the central cluster washing out the cavities. With the methods used in this paper, we have determined that cavities would be detectable to within 30°of rotation from the line of sight, and marginally detectable to within 20°of rotation. Cavities were not visible when directly aligned with the line-of-sight, though it is unclear if this would remain true with other methods of fitting.

4.5 Trials of Cavities with Randomized Orientations

For this experiment, three sets of trials were simulated – one at 50 kpc, one at 100, and one at 200 – with each set consisting of 10 images run with a 4ks observation time. In an attempt to simulate more realistic conditions, cavities were given a random orientation about the x, y, and z axes.

Once all of the trials were prepared, a visual inspection was conducted with DS9. Any images in which the cavities were difficult to see were labeled marginal detections, and were subsequently exported to Veusz. There residuals were created to check if the cavities were visible with any statistical significance. The results of these residuals are presented on the following page:

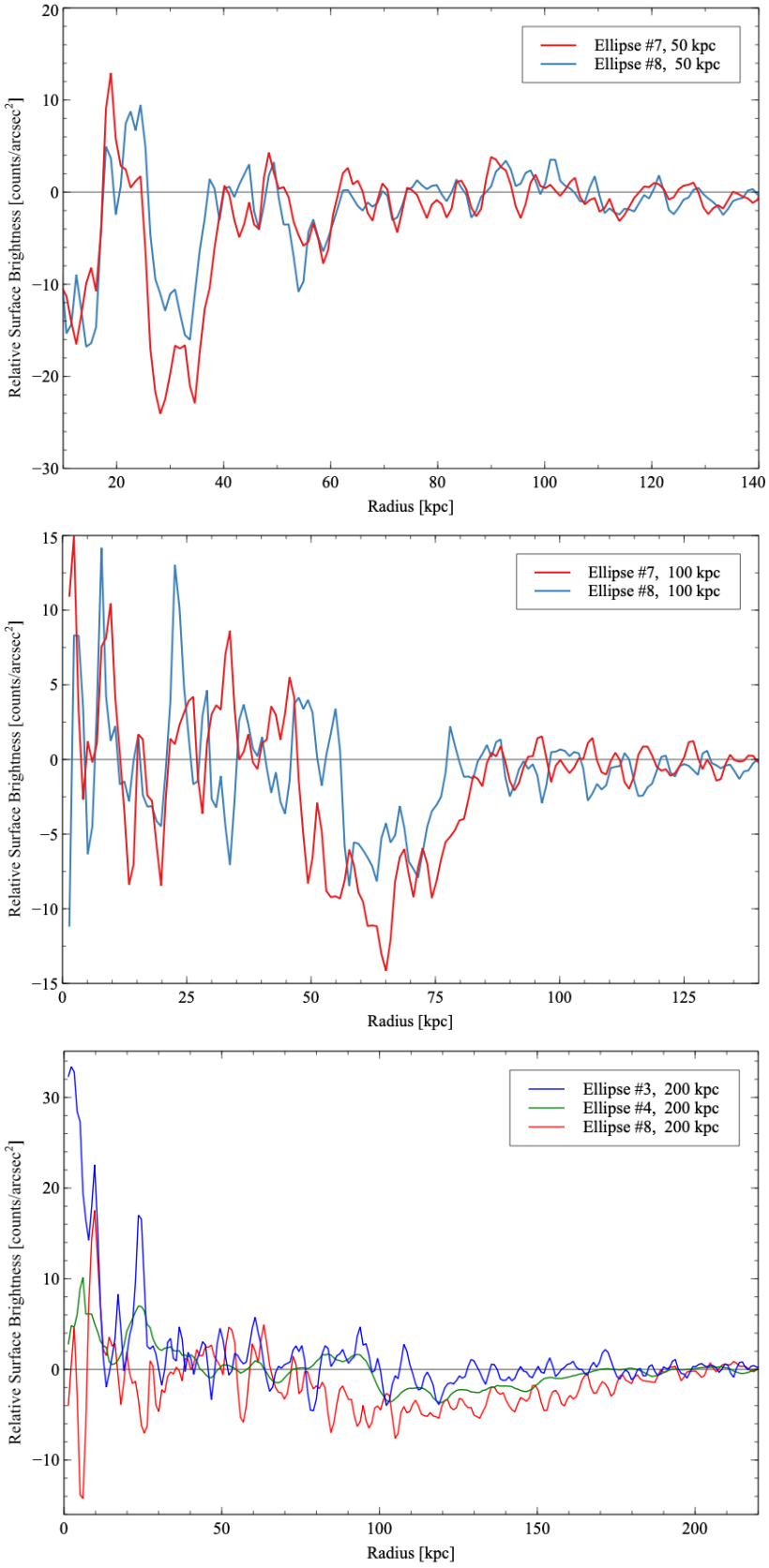

Figure 10: Residuals for marginal plots of 50, 100 and 200 kpc randomized trials. Note the general underestimation of size and shift of cavity centers to the left of the plot.

In both the 50 and 100 kpc trials, 2 marginals were exported to Veusz for analysis. Three marginals were flagged for analysis in the 200 kpc trials, by comparison, consistent with the increased difficulty of detection we would expect as the distance to the center increases. All marginal detections were able to produce statistically significant data with the exception of Ellipse #3 in the 200 kpc set, further supporting the increased difficulty of detection associated with the larger cavity distance.

Notably, all marginals show signs consistent with rotation near the line-of-sight, being both closer to the center of the cluster than anticipated and underestimated in size. The 50 kpc trials appear to be centered around 30 kpc, with a diameter of less than 20 kpc. Meanwhile, the 100 kpc trials appear to be centered around 65 kpc, with diameters in the rough vicinity of 20 – 35 kpc. Both of the detectable 200 kpc trials also appear both further to the right and smaller than expected, but of note in this set is Ellipse #4, which curiously appears centered farther out than Ellipse #8. This is inconsistent with previous data, where a lower magnitude of relative surface brightness typically corresponded with a cavity appearing closer to the cluster center. It may very well be the case, however, that this is due to the cavity's rotation about the x and y axes – the effects of these sorts of rotation on the apparent center of the cavity cluster were not considered during the orientation experiment.

5 Conclusions

Based on these experiments, we can arrive at a few useful conclusions. First, Lynx might be able to see cavities effectively out to 400 kpc; this would represent a marked improvement on current data, which has currently recorded cavities out to distances of only 200 kpc. Second, it may be possible to obtain useful data in most scenarios with observations as low as 4ks, as we saw in the cavity orientation and random trial experiments; this is once again a dramatic improvement on the median for Chandra observations of this kind of source, which sits around 40 ks. We also found that observations may become difficult if the cavities are within 30 degrees of our line-of-sight – or past around 70 degrees of rotation on the YZ plane – and our results were confirmed reasonably well by our randomized trials. However, it is possible that Lynx may be capable of yet finer detections, as our method of data analysis likely inhibited our ability to observe cavities very near to our line of sight.

Future work should focus on both increasing the complexity of the models used here to better mirror real world data and on increasing the number of trials used for each experiment. The impacts of non-spheroid cavities and clusters, proper spectrum or background noise models, and the existence of more than one pair of cavities simultaneously or cavities which may exist off-axis are all factors which further experimentation may address.

References

[Diehl et al., 2008] Diehl, S., Li, H., L. Fryer, C., and Rafferty, D. (2008). Constraining the nature of x-ray cavities in clusters and galaxies. *The Astrophysical Journal*, 687(1):173–192.

[Dunn and Fabian, 2006] Dunn, R. and Fabian, A. (2006). Investigating agn heating in a sample of nearby clusters. *Monthly Notices of the Royal Astronomical Society*, 373:959–971.

[Edge et al., 2000] Edge, A. C., Stewart, G. C., Fabian, A. C., and Arnaud, K. A. (2000). An x-ray flux-limited sample of clusters of galaxies : evidence for evolution of the luminosity function. *Annual Review of Astronomy and Astrophysics*, 38:289–335.

[Fabian, 2012] Fabian, A. C. (2012). Observational evidence of agn feedback. *Annual Review of Astronomy and Astrophysics*, 50:455–489.

[Gaskin et al., 2019] Gaskin, J. A., Swartz, D. A., Vikhlinin, A., Özel, F., Gelmis, K. E., Arenberg, J. W., Bandler, S. R., Bautz, M. W., Civitani, M. M., Domingues, A., Eckart, M. E., Falcone, A. D., Figueroa-Feliciano, E., Freeman, M. D., Günther, H. M., Havey, K. A., Heilmann, R. K., Kilaru, K., Kraft, R. P., McCarley, K. S., McEntaffer, R. L., Pareschi, G., Purcell, W., Reid, P. B., Schwartz, E. D., Tananbaum, H. D., Tremblay, G. R., Zhang, W. W., and Zuhone, J. A. (2019). Lynx x-ray observatory: an overview. *Journal of Astronomical Telescopes, Instruments, and Systems*, 5(2).

[McNamara and Nulsen, 2007] McNamara, B. and Nulsen, P. (2007). Heating hot atmospheres with active galactic nuclei. *Annual Review of Astronomy Astrophysics*, 45:117–175.

[Mulchaey, 2000] Mulchaey, J. S. (2000). 3.3. spatial properties of the intragroup medium. *Annual Review of Astronomy and Astrophysics*, 38:289–335.

[Vikhlinin et al., 2006] Vikhlinin, A., Kravtsov, A., Forman, W., Jones, C., Markevitch, M., Murray, S. S., and Van Speybroeck, L. (2006). Chandra sample of nearby relaxed galaxy clusters: Mass, gas fraction, and mass-temperature relation. *The Astrophysical Journal*, 640(2):640–691.

[Yamaguchi et al.,] Yamaguchi, H., Sato, K., and Smith, R. K. *SIMX Manual for ASTRO-H members*. Harvard.